Residues in the central β-hairpin of the DNA helicase of bacteriophage T7 are important in DNA unwinding

Ajit K. Satapathy, Anna B. Kochaniak, Sourav Mukherjee[2], Donald J. Crampton[3], Antoine van Oijen, and Charles C. Richardson[1]

Department of Biological Chemistry and Molecular Pharmacology, Harvard Medical School, 240 Longwood Avenue, Boston, MA 02115

Contributed by Charles C. Richardson, March 3, 2010 (sent for review December 30, 2009)

The ring-shaped helicase of bacteriophage T7 (gp4), the product of gene 4, has basic β-hairpin loops lining its central core where they are postulated to be the major sites of DNA interaction. We have altered multiple residues within the β-hairpin loop to determine their role during dTTPase-driven DNA unwinding. Residues His-465, Leu-466, and Asn-468 are essential for both DNA unwinding and DNA synthesis mediated by T7 DNA polymerase during leading-strand DNA synthesis. Gp4-K467A, gp4-K471A, and gp4-K473A form fewer hexamers than heptamers compared to wild-type helicase and alone are deficient in DNA unwinding. However, they complement for the growth of T7 bacteriophage lacking gene 4. Single-molecule studies show that these three altered helicases support rates of leading-strand DNA synthesis comparable to that observed with wild-type gp4. Gp4-K467A, devoid of unwinding activity alone, supports leading-strand synthesis in the presence of T7 DNA polymerase. We propose that DNA polymerase limits the backward movement of the helicase during unwinding as well as assisting the forward movement necessary for strand separation.

beta hairpin | DNA replication | leading-strand synthesis | oligomerization | sliding helicase

The replisome of bacteriophage T7 can be reconstituted using T7 gp5 (DNA polymerase), *Escherichia coli* thioredoxin (trx) (processivity factor), T7 gp2.5 (ssDNA-binding protein) and T7 gp4 (helicase-primase) (1). The helicase domain of gp4 places it within the SF4 family of helicases (2). Like other members of this family, gp4 assembles onto ssDNA as a hexamer, an oligomerization that is facilitated by dTTP (3, 4). The inherent dTTPase of gp4 is stimulated approximately 40-fold by ssDNA, a stimulation that is required for its unidirectional translocation on ssDNA (4, 5). However, the molecular mechanism by which ssDNA enhances the hydrolysis of dTTP is not well understood. Although gp4 alone translocates on ssDNA and catalyzes limited unwinding of dsDNA, its major role in replication is manifest when it functions with T7 DNA polymerase within the replisome (1, 6). DNA synthesis activity of gp5/trx provides the driving force to accelerate DNA unwinding by gp4 (7). The association of gp5/trx with gp4 during leading-strand DNA synthesis increases the processivity for the 800 nucleotides observed using ssDNA templates to greater than 17 kb per binding event (1).

The crystal structure of the hexameric gp4 shows a 6-fold symmetric ring with a central core of 25–30 Å, dimensions that resemble the size and shape of the gp4 hexameric rings seen in electron micrographs (3, 8). Electron microscopy combined with other studies provides strong evidence that the ssDNA passes through the central core that provides the DNA-binding site. It is proposed that ssDNA transfers from one subunit to the adjacent subunit sequentially (8, 9). The crystal structure of gp4 also revealed the presence of three loops (loops I, II, and III) that protrude into the central cavity (8). Earlier mutational data had suggested that residues around loop I (residues 424–439) and loop II (residues 464–475) interact with ssDNA (10, 11). These loops not only extend into the central cavity but they also contain a number of basic residues suitable for binding the negatively charged phosphate backbone of the ssDNA. Of these loops, loop II emanates from helicase motif III and ends with helicase motif IV forming a β-hairpin structure (Fig. 1*A*). The amino acid residues from position 465–475 are well conserved in a few other hexameric helicases (Fig. 1*B*). The β-hairpin is analogous to the mobile loop L2 of *E. coli* RecA and the DNA-binding β-hairpin of replicative hexameric helicases of SV40, bovine papiloma viruses, and *E. coli* (12–15). The β-hairpin has three lysine residues and an asparagine that are candidates for electrostatic interaction with the negatively charged backbone of DNA. A genetically altered gp4 with substitutions for all three lysine residues (Lys-467, Lys-471, and Lys-473) shows no significant hydrolysis of dTTP, ssDNA binding, and dsDNA unwinding activities in vitro (9).

In the present study, we have altered eight amino acid residues in the central β-hairpin region of T7 gp4. The genetic and biochemical properties of the gp4 variants are analyzed in isolation or in association with T7 gp5/trx to envisage the role of the helicase under physiological circumstances. Our results reveal critical roles of several of these residues in unwinding of DNA by the helicase. One of the altered helicases is devoid of unwinding activity alone but nevertheless can support leading-strand DNA synthesis in conjunction with the polymerase.

Results

In vivo Analysis of Alterations in the β-hairpin of Gene 4 Helicase. In order to explore the relevance of each amino acid residue in the β-hairpin loop, the residues at positions from 465 to 473 were substituted with alanine. The resulting constructs were transferred to *E. coli* strain C_{600} and then tested for their ability to complement T7Δ4 phage lacking gene 4 for growth. The results show that gp4-H465A, gp4-L466A, and gp4-N468A do not support the growth of T7Δ4 phage (Table S1). However, plasmids encoding for gp4-K467A, gp4-P469A, gp4-D470A, gp4-K471A, and gp4-K473A complement the growth of T7Δ4 phage as well as wild-type gene 4. His-465 cannot be replaced with any other amino acid without a loss of function; however, Leu-466 can be replaced by hydrophobic residues such as isoleucine, valine, or cysteine. These results suggest that the central β-hairpin plays an essential role in T7 helicase function, with His-465, Leu-466, and Asn-468 being critical for function.

β-Hairpin Residues Affect ssDNA-Dependent dTTP Hydrolysis. In the absence of ssDNA, gp4 hydrolyzes dTTP poorly (V_{max}: 0.4 μM $\cdot$ s^{-1}) but the rate of hydrolysis increases approximately 40-fold

Author contributions: A.K.S. and D.J.C. designed research; A.K.S., A.B.K., S.M., and D.J.C. performed research; A.K.S., A.B.K., D.J.C., A.M.v.O., and C.C.R. analyzed data; and A.K.S., D.J.C., A.M.v.O., and C.C.R. wrote the paper.

The authors declare no conflict of interest.

[1]To whom correspondence should be addressed. E-mail: ccr@hms.harvard.edu.

[2]Present address: Sun Pharmaceutical Industries Ltd., Vadodara 390020, Gujarat, India.

[3]Present address: Department of Chemistry and Biochemistry, Clark University, Worcester, MA 01602.

This article contains supporting information online at www.pnas.org/cgi/content/full/1002734107/DCSupplemental.

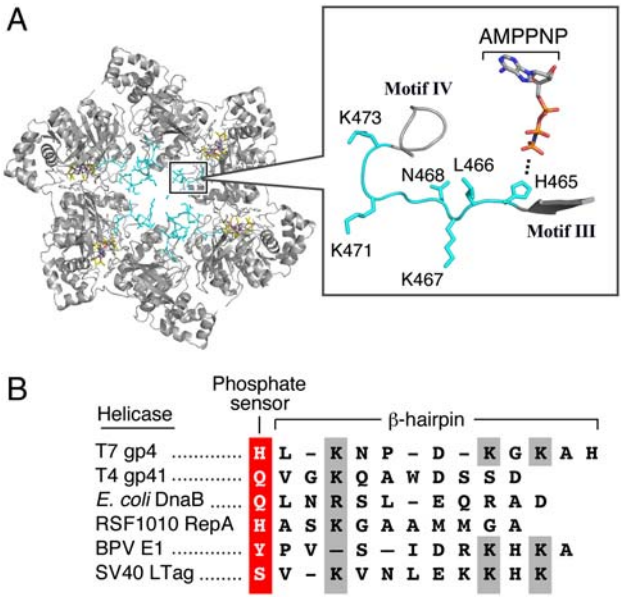

Fig. 1. Location and alignment of the β-hairpin of gp4. (*A*) The crystal structure of the helicase domain of T7 gp4 (8) (Protein Data Bank accession no. 1E0K) drawn in Pymol. The location of the β-hairpin structure of loop II between the helicase motif III and motif IV from a single subunit is shown in the box and a few important amino acid residues located in the β-hairpin, relevant for this study, are depicted in the magnified picture. (*B*) Homologous alignment of the amino acid residues located in the central β-hairpin structure in different hexameric helicases. The phosphate sensor (His-465 in T7 gp4), and the conserved basic residue (Lys-467 in T7 gp4) in the region are highlighted. Note that BPV E1 and SV40 LTag are SF3 helicases, whereas others are SF4 helicases.

in the presence of ssDNA (V_{max}: 13.4 μM · s^{-1}). The wild type and the altered gp4 were purified as described previously (9). The purity was greater than 95% as judged by Coomassie staining of proteins after SDS gel electrophoresis. The proteins were examined for their ability to hydrolyze dTTP. All the gp4 variants exhibit similar rates of dTTP hydrolysis (V_{max}: 0.2–0.4 μM · s^{-1}) in the absence of ssDNA (Table S2). However, the hydrolysis of dTTP catalyzed by gp4-H465A, gp4-L466A, and gp4-N468A is not stimulated by the presence of ssDNA. The stimulation in ssDNA-dependent hydrolysis catalyzed by gp4-K467A, gp4-P469A, gp4-D470A, gp4-K471A, and gp4-K473A is about 15–45% of that observed with wild-type helicase (Table S2). Notably, gp4-K467A, which exhibits only 15% of the wild-type dTTPase activity, is able to support the growth of T7Δ4.

Effect of Alteration in the β-Hairpin of Gp4 on Binding to DNA and on Unwinding Duplex DNA. We measured the ability of each protein to bind to ssDNA in the presence of the nonhydrolyzable analog β, γ-methylene dTTP using a nitrocellulose DNA-binding assay (Fig. 2*A*). The dissociation constants of wild-type and variant gp4s for a 50-mer oligonucleotide are shown in Table S3. Wild-type gp4 binds the oligonucleotide with a dissociation constant of 26 nM. Under similar conditions, gp4-L466A and gp4-N468A have low affinity for the ssDNA such that the dissociation constants could not be determined (Fig. 2*A*). Gp4-H465A, gp4-D470A, gp4-K471A, and gp4-K473A bind the 50-mer oligonucleotide 2-fold weaker with dissociation constants (kDs) of 41–47 nM. Gp4-K467A has a 10-fold lower affinity for the oligonucleotide (kD: 200 nM) relative to the wild-type gp4. We have also observed the affinity of gp4-K467A (Km-4 nM) for ssM13DNA is about 7 folds weaker than compared with wild-type gp4 (Km-0.6 nM) in dTTP hydrolysis assay (Fig. S1). These results suggest that the reduced level (15% of wild-type gp4) of hydrolysis of dTTP in the presence of ssDNA observed with gp4-K467A arises from its lower affinity for ssDNA.

Further, we used a short duplex DNA (see the inset of Fig. 2*B*) to measure the DNA unwinding activity of the proteins. In our experimental conditions, gp4-H465A, gp4-L466A, and gp4-N468A did not exhibit any significant level of DNA unwinding (Fig. 2 *B* and *C*). However, gp4-D470A, gp4-K471A, and gp4-K473A retained up to 30% of the activity measured with the wild-type enzyme. Gp4-P469A unwinds the dsDNA substrate as well as does wild-type gp4. Notably, gp4-K467A, which complements the gene 4 functions in vivo, unwinds DNA poorly and exhibits less than 5% of the wild-type activity.

Leading-Strand DNA Synthesis Mediated by Gp5/trx and Gp4. Gp5/trx catalyzes processive DNA synthesis on ssDNA templates, but is unable to catalyze strand-displacement DNA synthesis on duplex DNA. However, the two enzymes, gp4 and gp5/trx, together mediate extensive leading-strand synthesis (16, 17). We have examined the ability of the various gp4 to mediate leading-strand synthesis with gp5/trx. In this assay, we have used circular double-

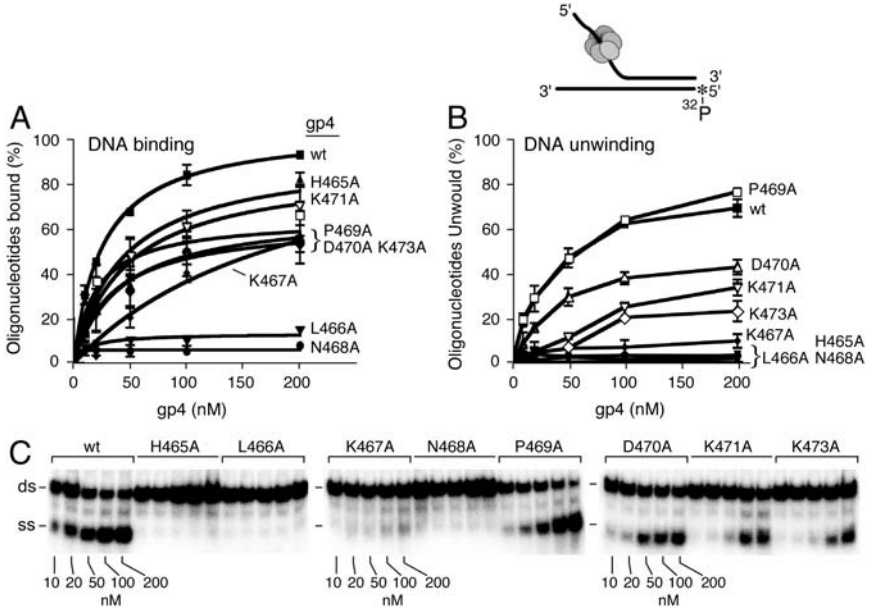

Fig. 2. ssDNA binding and dsDNA unwinding activity of gene 4 proteins. (*A*) Ability of gp4 variants to bind a 50-mer oligonucleotide was measured in a nitrocellulose filter binding assay. Error bars represent the standard deviation of three independent experiments. (*B*) Ability of gp4 variants to unwind dsDNA. The dsDNA unwinding activity of gp4 was measured using a DNA substrate (depicted in the inset) consisting of a 5′-^{32}P-labeled 75-mer oligonucleotide that is partially annealed to a 95-mer oligonucleotide. The substrate has 56 base pairs complementary region with a 39 nucleotides 5′ and 19 nucleotides 3′ overhang. After incubation for 10 min at 37 °C the reaction sample was loaded onto a 10% nondenaturing gel. The amount of unwound DNA separated from the duplex DNA substrate by gp4 was determined using a phosphor imager. Error bars represent the standard deviation of three independent experiments. (*C*) Gel analysis of products of unwinding of DNA. The gel photograph shows a representative picture of the unwinding reactions carried out by gp4 variants. The gel shows the separation of unwound ssDNA from the dsDNA substrate in a 10% nondenaturing gel.

BIOCHEMISTRY

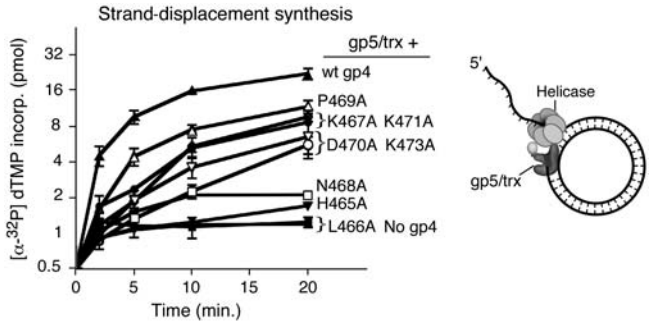

Fig. 3. Leading-strand DNA synthesis mediated by gp5/trx and gp4. DNA synthesis mediated by gp5/trx and gp4 was measured in an assay containing 10 nM M13 double-stranded DNA with a 5′-ssDNA tail on the interrupted strand as depicted in the inset, 0.5 mM dATP, dCTP, dGTP, [α-^{32}P] dTTP (0.1 μCi), 10 nM gp5/trx, and 20 nM hexamer of the indicated helicase. After incubation for the indicated time periods at 37 °C, the reactions were stopped by the addition of EDTA to 25 mM final concentration. The DNA synthesis activity is expressed in terms of the quantity of [α-^{32}P] dTMP incorporated as measured by liquid scintillation counting and plotted using Graphad prism software. The *y* axis is plotted in log 2 scale. Error bars represent the standard deviation of three independent experiments.

stranded DNA bearing a 5′-ssDNA tail onto which gp4 can assemble (see Fig. 3 *Inset*). As anticipated, wild-type gp4 enables gp5/trx to mediate leading-strand synthesis (Fig. 3). Gp4-H465A, gp4-L466A, and gp4-N468A do not support leading-strand DNA synthesis activity. This result may be due to their inability to catalyze nucleotide hydrolysis and DNA unwinding. In addition, it cannot be ruled out that these proteins fail to interact with the polymerase and this impedes their ability to participate in this reaction. Surprisingly, gp4-K467A, which hydrolyzes dTTP at a reduced rate (V_{max}: 1.4 μM · s^{-1}), performs a significant level of leading-strand DNA synthesis in association with gp5/trx (Fig. 3). Gp4-P469A, gp4-D470A, gp4-K471A, and gp4-K473A also support leading-strand DNA synthesis, albeit at a reduced rate (30–50%) as compared to wild-type gp4. The ability of gp4-K467A to support leading-strand synthesis is discussed below.

DNA Unwinding and dTTP Hydrolysis During Leading-Strand Synthesis Mediated by Gp5/trx and Gp4. We used a minireplication fork (depicted in Fig. 4*A*), which provides loading sites for both helicase and polymerase and can be used to measure the unwinding of DNA that accompanies leading-strand synthesis. In this assay, we have used gp5-Exo$^-$/trx to avoid the degradation of unwound strands (18). Wild-type gp4 alone displayed a limited ability to displace the labeled strand (Fig. 4*C*). The reason behind such weak unwinding by gp4 may be the presence of the short primer (23nt) which prevents the helicase from interacting with the excluding strand (19). gp5-Exo$^-$/trx alone catalyzes some strand-displacement (Fig. 4 *B* and *C*), an anticipated result since gp5/trx lacking exonuclease activity has been shown to catalyze limited strand-displacement synthesis (16). Our experimental results also show that wild-type gp4 and gp4-K467A, gp4-K471A, and gp4-K473A (K → $A_{\beta\text{-hairpin loop}}$ proteins) unwind the minireplication fork in association with DNA synthesis catalyzed by gp5-Exo$^-$/trx. This finding may explain the strand-displacement DNA synthesis activity mediated by gp4 K → $A_{\beta\text{-hairpin loop}}$ proteins seen in Fig. 3.

We have also measured the rate of dTTP hydrolysis by gp4 variants in association with the gp5/trx on M13 ssDNA and M13 dsDNA (Fig. S2). We did not observe any significant difference in the rate of dTTP hydrolysis by the wild-type gp4 or other gp4 variants in association with the gp5/trx on M13 ssDNA. However, we observed a modest increased rate of dTTP hydrolysis on M13 dsDNA in similar reaction conditions. In the latter case, DNA synthesis was coupled to the DNA unwinding in the presence of all four dNTPs. The results demonstrate that the unwinding activity of Gp4-K467A is increased up to 50% of the wild type in association with gp5/trx (Fig. 4 *B* and *C*), however, the rate of dTTP hydrolysis for gp4-K467A is much reduced compared to the wild-type protein, but perhaps this is sufficient for unwinding of the DNA ahead of the advancing DNA polymerase. This result leads us to speculate that the polymerase enhances the unwinding by the helicase at low cost of energy utilization during strand-displacement synthesis.

Gp4 K → $A_{\beta\text{-hairpin loop}}$ Proteins are Defective in Forming Hexamers in the Presence of DNA. Gp4 K → $A_{\beta\text{-hairpin loop}}$ variants bind poorly to oligonucleotides (Table S3). In order to investigate the reason behind their weak DNA binding, we examined their ability to oligomerize, a prerequisite for DNA binding. In the experiment presented in Fig. 5, we have determined the ability of the gene 4 proteins to form hexamers and heptamers in the presence of a 50-mer oligonucleotide and β, γ-methylene dTTP as previously described (20). In this assay, the altered proteins, gp4-K467A, gp4-K471A, and gp4-K473A formed more heptamers than hexamers as compared to the wild-type gp4. It was previously reported that only hexamers, not heptamers, bind ssDNA (20).

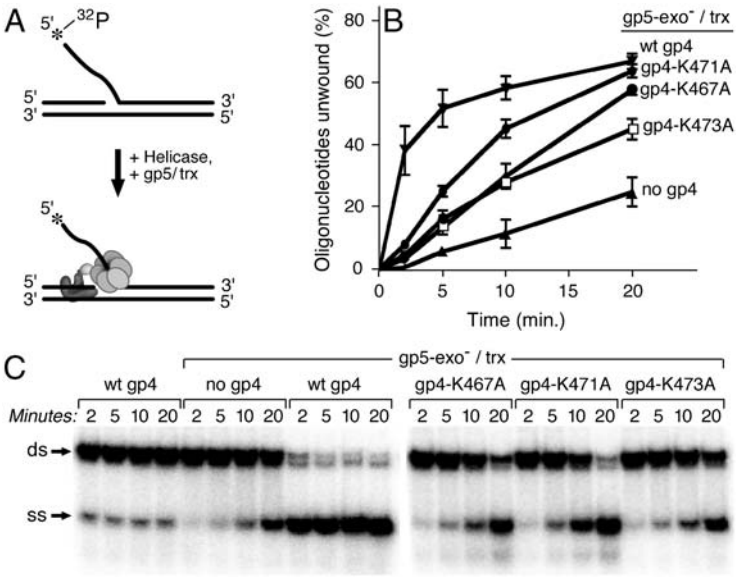

Fig. 4. T7 gp5/trx enhances unwinding of DNA by wild-type gp4 and loop II variants of gp4. (*A*) The minireplication fork depicted was prepared by annealing a short primer of 23-mer oligonucleotide to the 3′-end of a 54-mer oligonucleotide to which had been annealed a 66-mer oligonucleotide bearing a displaced ssDNA tail with a 5′-^{32}P. The substrate has loading sites for both helicase and polymerase. (*B*) DNA unwinding activity of wild-type gp4, gp4-K467A, gp4-K471A, and gp4-K473A in association with T7 gp5-Exo$^-$/txt. In this assay, we have used the minireplication fork depicted in *A*. Error bars represent the standard deviation of three independent experiments. (*C*) The gel photograph shows a representative picture of the unwinding reactions carried out by gp4 variants in association with gp5-Exo$^-$/txt.

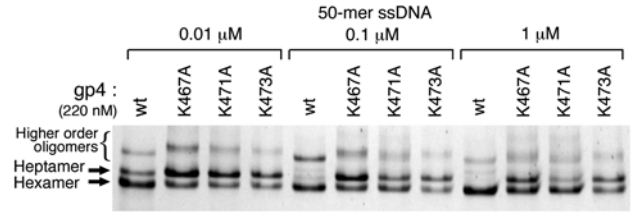

Fig. 5. K → $A_{\beta\text{-hairpin loop}}$ proteins defective in forming hexamers in the presence of DNA. Oligomerization assay for wild-type and altered gp4 in the presence of the indicated concentrations of 50-mer ssDNA were carried out as described by Crampton et al. (20). Reactions were carried out in 20 μL volume containing 220 nM (hexamer) wild-type or altered gp4, 5 mM β, γ-methylene dTTP, and 50-mer ssDNA. After incubation at 37 °C for 20 min, glutaraldehyde was added at 0.033% and further incubated for 5 min at 37 °C then loaded onto a 10% nondenaturing gel. The state of oligomerization of the proteins was determined after staining the gel with Coomassie blue.

Thus, the results suggest that the lysine residues in the central β-hairpin play a role in the ability of gp4 to convert from heptamers to hexamers. Gp4-N468A binds ssDNA poorly (Fig. 2*A*). These results, taken together, suggest that the basic residues, namely, Lys-467, Asn-468, Lys-471, and Lys-473, play a major role for the function of the β-hairpin loop II in recruiting ssDNA in the central core of the hexameric ring of T7 helicase.

Single-Molecule Analysis of Leading-Strand Synthesis Mediated by Gp5/trx and Gp4 Variants. The results so far presented show that gp4-K467A complements T7Δ4 phage growth and mediates leading-strand synthesis in association with gp5/trx. However, the gp4 variant is significantly defective in ssDNA binding, ssDNA-dependent dTTP hydrolysis, as well as ssDNA-dependent hexamerization and DNA unwinding. Because gp4-K467A forms fewer hexamers, we might observe leading-strand synthesis mediated by a fraction of the proteins used in the reactions. These possibilities are difficult to address with ensemble averaging experiments. Therefore we have examined leading-strand synthesis mediated by gp4-K467A using single-molecule techniques.

The procedure for the leading-strand synthesis assay using single-molecule techniques was followed as described by Lee et al. (6) with a slight modification (Fig. 6 *A* and *B*). Bead-bound and surface-tethered DNA were preincubated with T7 gp5/trx and T7 gp4 in replication buffer with dNTPs for 15 min. Next, the flow cell was washed with 15 flow cell volumes of replication buffer with dNTPs. Decreasing the wash time was found to improve yield of observed primer extension events, thus increasing throughput, with the gp4 mutants. Typically, wild-type gp4 and gp4-K471A experiments were carried out with 15 flow cell volumes of washes, whereas only three flow cell volumes were used for gp4-K467A and gp4-K473A. Finally, DNA synthesis was initiated by introducing replication buffer with dNTPs and $MgCl_2$. From the data presented in Fig. 6*C*, the rate of leading-strand synthesis mediated by gp5/trx and wild-type gp4 is 155 ± 9 bp/s ($n = 35$) in good agreement with the previous results (6, 21). Gp4 K → $A_{\beta\text{-hairpin loop}}$ variants (gp4-K467A, gp4-K471A, and gp4-K473A) were also able to support wild-type rates of strand-displacement synthesis (Fig. 6*C*). The finding that these variants, especially gp4-K467A, support strand-displacement synthesis at 175 ± 11 bp/s ($n = 20$) as well as does the wild-type protein supports our biochemical and genetic results. However, the relative number of observed replication events for gp4-K467A seems to be significantly lowered as compared to wild-type protein, provided by the fact that we had to lessen the stringency of the wash between preassembly and activation of the helicase and polymerase activities with $MgCl_2$ to see these replication events. We speculate that the decreased number of events could arise from only a fraction of the proteins used in this assay forming hexamers as evidenced in Fig. 5 and their assembling with gp5/trx; however, we were unable to obtain the statistical information pertaining to this speculation in single-molecule experiments.

Discussion

In the present study, we have focused on the β-hairpin loop of the T7 helicase, a loop that is physically located in the central core of the hexameric protein. The β-hairpin loop is located between helicase motifs III and IV. The location of this loop and its basic charge make it a likely candidate for a role in the binding of ssDNA. Such a role is supported by studies on the corresponding DNA-binding β-hairpin loops from other hexameric helicases including SV40 LTag, UvrB, and BPV E1 (13, 22, 23). Altering residues His-465, Leu-466, and Asn-468 of the β-hairpin of the T7 helicase has the greatest effect on helicase associated activities as compared to the other residues in the loop. It seems likely that these three residues either play a critical role in the structure of the

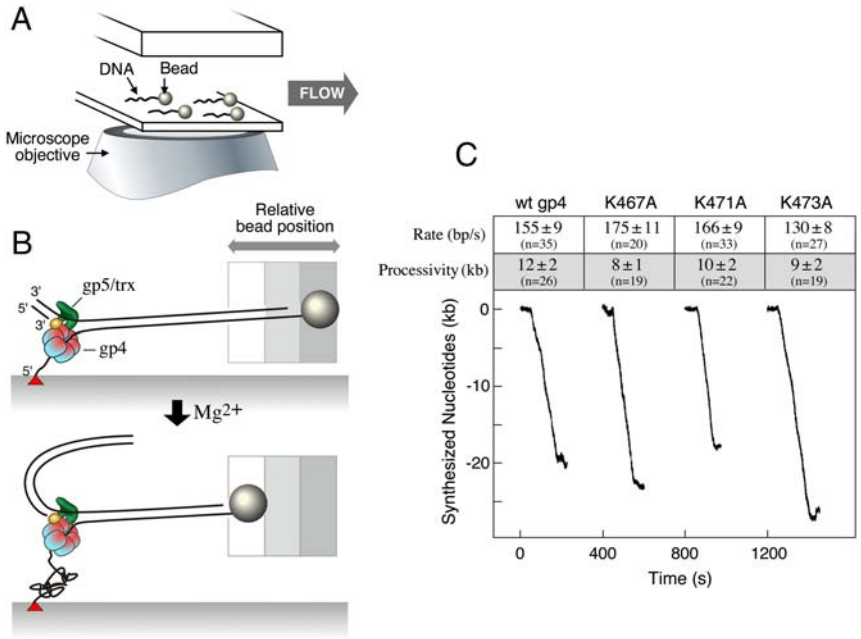

Fig. 6. Single-molecule microscopy of leading-strand synthesis. (*A*) Schematic representation of the experimental arrangement as described by Lee et al. 6. Phage lambda DNA molecules bearing a replication fork at one end are attached to the glass surface of a flow cell and by the other end to a bead. The flow cells were placed on an inverted microscope and the beads were imaged using a digital CCD camera. (*B*) Duplex lambda DNA (48.5 kb) is attached to the surface of the flow cell via one of the 5′-end of the fork using biotin-streptavidin interaction, the 3′-end of the same strand is attached to a paramagnetic bead using digoxigenin-anti-digoxigenin interaction. Gp5/trx and gp4 are preassembled at the replication fork in the presence of dNTPs. The reaction is started by the addition of $MgCl_2$ and dNTPs. The positions of the beads are recorded and analyzed as described in *Methods*. (*C*) Rate and processivity of strand-displacement synthesis of T7 gp5/trx associated with the wild-type or altered gp4. Examples of single-molecule trajectories for strand-displacement synthesis are shown. Rate and processivity is calculated by fitting the distributions of individual single-molecule trajectories using Gaussian and exponential decay distributions, respectively. Values represent the mean with the standard of the mean as error.

β-hairpin loop and/or the coupling of DNA binding to the hydrolysis of dTTP. In T7 gp4, the central β-hairpin loop emanates from His-465, which interacts with the γ-phosphate of the bound NTP and is involved in phosphate sensing (20, 24). The adjacent residue Leu-466 can be replaced by a few highly hydrophobic residues for the function of gp4 in phage growth suggesting that substitution of Leu-466 with alanine or less hydrophobic residues might perturb the mechanical link between the β-hairpin loop and the nucleotide-binding site.

Examination of the central cavity of a hexameric crystal structure of the T7 helicase reveals a potential DNA-binding "groove" formed by the β-hairpin loops (Fig. S3). However, such a positive electrostatic groove is discontinuous in the heptameric structure (8, 25). It is likely that this architectural difference prevents the heptamer from binding DNA within the central cavity as observed in biochemical analyses (20). Oligomerization assays show that the basic residues Lys-467, Asn-468, Lys-471, and Lys-473 are important for gp4 in forming hexamers. Formation of a productive helicase–nucleic acid complex is a crucial rate-limiting step in the DNA unwinding mechanism of T7 helicase (26). Our results show that substitution of these basic residues with alanine leads to a decrease in the affinity for ssDNA and in the unwinding of DNA. We propose that the basic residues in the central β-hairpin play a role in recruiting ssDNA into the central channel and that they are important in conveying the occupancy of the loop to the catalytic site, probably through His-465. This communication allows for the activation of dTTP hydrolysis in the presence of ssDNA. The exact mechanism of ring-opening is not clear from this study. It has been proposed that heptamers lose one subunit in the process of encircling the DNA (20). A similar mechanism has been proposed for RuvB protein in which the loss of a subunit from the heptamer accompanies binding to dsDNA (27).

A fundamental feature of hexameric helicases is the adoption of staircase architecture by the β-hairpin loops through a set of interactions involving a basic and acidic residue from adjacent subunits (28). The crystal structure of gp4 reveals such an interaction of β-hairpin loops through Lys-467 and Asp-470 of adjacent subunits in hexameric gp4 (Fig. S3). However, such spiral staircase architecture is missing from the heptameric gp4. It seems likely that Lys-467 is the most important player in the formation of this negatively charged cluster in the central channel, as evidenced from the conserved nature of a lysine residue in similar position of central β-hairpins from other hexameric helicases (Fig. 1*B*). This residue also lines the wall of the groove formed in the hexameric gp4 (Fig. S3). The substitution of Asp-470 with alanine does affect the helicase associated functions of gp4, but nonetheless the helicase retains nearly 25–40% of the wild-type activity. Therefore, we believe Lys-467 has another interacting partner from the neighboring subunit, a partner that is yet to be revealed. It was shown previously that interactions of Asn-468 of loop II and Arg-493 of helicase motif IV from the adjacent subunit are critical for interactions with DNA (29). Some of the other residues in helicase motif IV implicated in DNA-binding are Arg-487 (10, 11) and Gly-488 (11), also found to line the DNA-binding groove and are in close proximity to Lys-467 in the crystal structure.

A dynamic interaction between gp4 and gp5/trx increases the rate and processivity of leading-strand DNA synthesis (21). The results obtained with gp4-K467A support a "Brownian" ratchet mechanism (Fig. 7) that has been proposed for other helicases (30, 31). In gp4-K467A, dTTP hydrolysis is nearly uncoupled from DNA unwinding. Our finding that gp4-K467A performs like wild-type helicase during strand-displacement synthesis with a marginal difference in the rate and processivity of DNA synthesis supports a model in which gp5/trx acts to limit backward movement of the helicase (Fig. 7). Evidence for backward movement of the helicase was found previously from identification of an altered protein that has a higher ratio of DNA unwinding to

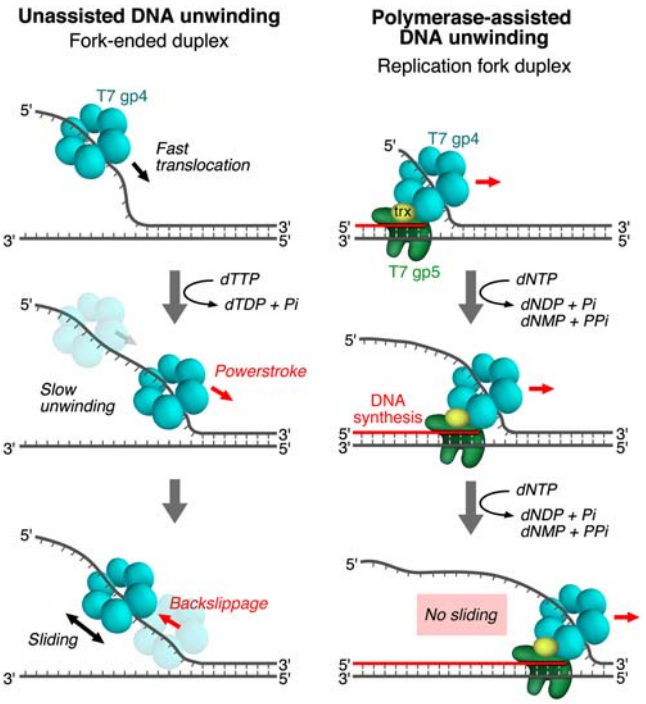

Fig. 7. Unassisted versus assisted DNA unwinding byT7 gp4. The hexameric gp4 alone translocates on ssDNA from 5′-3′ direction coupled with NTP hydrolysis. Once gp4 finds a double-strand junction, its translocation speed weakens and with NTP hydrolysis it destabilizes a region of dsDNA near the junction and translocates slowly because of the hindrance caused by the complimentary strand. In the process of nucleotide release, helicase may undergo back slippage because of sliding by Brownian motion. The slow unwinding of a fork-ended duplex by an unassisted gp4 is the effect of its dTTPase-driven duplex destabilization and back slippage. However in the gp5/trx assisted reactions, both gp5/trx and gp4 together perform strand-displacement synthesis on replication fork substrate, where translocation of gp4 and DNA synthesis by gp5/trx collectively destabilizes the dsDNA junction and gp4 passively traps the displaced strand leads to no further decrease in the helicase associated translocation speed. The rate of DNA synthesis by gp5/trx maintains the translocation rate of gp4. The faster unwinding of a replication fork by an assisted gp4 is a result of the total effect of the duplex destabilization by gp5/trx and gp4, the directional translocation, and prevention of back slippage of gp4 by gp5/trx.

dTTP hydrolysis (32). Any backward movement of the helicase will be reduced by the presence of the DNA polymerase, thus enhancing the unwinding of DNA (7). Not surprisingly, movement of gp5/trx in the 5′-3′ direction during DNA synthesis and its physical interaction with gp4 pushes the latter in the same direction. Our results show that pushing of the gp4 by gp5/trx is able to augment DNA unwinding if the helicase can slide on DNA. Such a polymerase pushing effect is proposed for T4 gp41 and *E. coli* DnaB (33, 34). We propose that gp4-K467A represents a "sliding" conformational form of the helicase that relies on gp5/trx to push it forward, substituting for the dTTPase-driven power-stroke of the helicase. However, recent studies have shown in the absence of the gp5/trx, gp4 unwinds DNA through a partially active mechanism (35). Gp4-K467A, devoid of unwinding activity alone, supports leading-strand synthesis in the presence of T7 DNA polymerase suggests a passive mechanism for DNA unwinding by gp4-K467A when it is coupled with T7 DNA polymerase.

Materials and Methods

Genetic and Biochemical Bulk Assay for Wild Type and Variants of Gp4. Phage complementation assay, ssDNA-dependent and independent dTTP hydrolysis assay, ssDNA-binding assay, dsDNA unwinding assay, protein oligomerization assay, and leading-strand DNA synthesis assay were performed as described in previously (36). Details of assay procedures can be found in the *SI Text*.

Single-Molecule Microscopy. Single-molecule leading-strand DNA synthesis assays were performed as described by Lee et al. 6. Phage lambda DNA molecules bearing a replication fork at one end are attached to the glass surface of a flow cell and by the other end to a bead (see Fig. 6). The flow cells were placed on an inverted microscope and the beads were imaged using a digital CCD camera. Typically, an area of 850×850 μm was imaged with a time resolution of 200 ms. Particle-tracking software (Semasopht) was then used to determine the center position of every bead for every frame with a precision of 10 nm. About 100 individual, tethered DNA molecules can be observed simultaneously, allowing for a high data throughput.

Bead-bound and surface-tethered DNA were preincubated with 20 nM T7 gp5/trx and 20 nM T7 gp4 (wild-type gp4, gp4-K467A, gp4-K471A, or gp4-K473A) in replication buffer (40 mM Tris 7.5, 50 mM potassium glutamate, 2 mM EDTA, 0.1 mg/mL BSA) with 700 μM each dNTP and 10 mM DTT for 15 min. Next, the flow cell was washed with replication buffer with dNTPs and DTT. Finally, DNA synthesis was initiated by introducing replication buffer with dNTPs, DTT, and 10 mM $MgCl_2$. After particle tracking, traces were corrected for residual instabilities in the flow by subtracting traces corresponding to tethers that were not enzymatically altered. Bead displacements were converted into numbers of nucleotides synthesized, using the known length difference between ssDNA and dsDNA at our experimental conditions (6). The resultant traces were smoothed and fitted with series of line segments to determine rates.

ACKNOWLEDGMENTS. We thank Masateru Takahashi and Arek Kulczyk for providing gp5 and $gp5^{EXO-}$/trx. We are grateful to all the members of the Charles Richardson lab for helpful discussions and constructive comments. We thank Steven Moskowitz (Advanced Medical Graphics) and Joseph Lee for illustrations and special thanks to Seung Joo Lee and Samir Hamdan for critical comments. This work was supported by a grant from the National Institutes of Health Grant GM54397 to C.C.R.

1. Hamdan SM, Richardson CC (2009) Motors, switches, and contacts in the replisome. *Annu Rev Biochem* 78:205–243.
2. Singleton MR, Dillingham MS, Wigley DB (2007) Structure and mechanism of helicases and nucleic acid translocases. *Annu Rev Biochem* 76:23–50.
3. Egelman EH, Yu X, Wild R, Hingorani MM, Patel SS (1995) Bacteriophage T7 helicase/primase proteins form rings around single-stranded DNA that suggest a general structure for hexameric helicases. *Proc Natl Acad Sci USA* 92:3869–3873.
4. Kim DE, Narayan M, Patel SS (2002) T7 DNA helicase: A molecular motor that processively and unidirectionally translocates along single-stranded DNA. *J Mol Biol* 321:807–819.
5. Tabor S, Richardson CC (1981) Template recognition sequence for RNA primer synthesis by gene 4 protein of bacteriophage T7. *Proc Natl Acad Sci USA* 78:205–209.
6. Lee JB, et al. (2006) DNA primase acts as a molecular brake in DNA replication. *Nature* 439:621–624.
7. Stano NM, et al. (2005) DNA synthesis provides the driving force to accelerate DNA unwinding by a helicase. *Nature* 435:370–373.
8. Singleton MR, Sawaya MR, Ellenberger T, Wigley DB (2000) Crystal structure of T7 gene 4 ring helicase indicates a mechanism for sequential hydrolysis of nucleotides. *Cell* 101:589–600.
9. Crampton DJ, Mukherjee S, Richardson CC (2006) DNA-induced switch from independent to sequential dTTP hydrolysis in the bacteriophage T7 DNA helicase. *Mol Cell* 21:165–174.
10. Notarnicola SM, Park K, Griffith JD, Richardson CC (1995) A domain of the gene 4 helicase/primase of bacteriophage T7 required for the formation of an active hexamer. *J Biol Chem* 270:20215–20224.
11. Washington MT, Rosenberg AH, Griffin K, Studier FW, Patel SS (1996) Biochemical analysis of mutant T7 primase/helicase proteins defective in DNA-binding, nucleotide hydrolysis, and the coupling of hydrolysis with DNA unwinding. *J Biol Chem* 271:26825–26834.
12. Story RM, Steitz TA (1992) Structure of the recA protein-ADP complex. *Nature* 355:374–376.
13. Shen J, Gai D, Patrick A, Greenleaf WB, Chen XS (2005) The roles of the residues on the channel beta-hairpin and loop structures of simian virus 40 hexameric helicase. *Proc Natl Acad Sci USA* 102:11248–11253.
14. Enemark EJ, Joshua-Tor L (2006) Mechanism of DNA translocation in a replicative hexameric helicase. *Nature* 442:270–275.
15. Wang G, et al. (2008) The structure of a DnaB-family replicative helicase and its interactions with primase. *Nat Struct Mol Biol* 15:94–100.
16. Lechner RL, Engler MJ, Richardson CC (1983) Characterization of strand displacement synthesis catalyzed by bacteriophage T7 DNA polymerase. *J Biol Chem* 258:11174–11184.
17. Lechner RL, Richardson CC (1983) A preformed, topologically stable replication fork. Characterization of leading strand DNA synthesis catalyzed by T7 DNA polymerase and T7 gene 4 protein. *J Biol Chem* 258:11185–11196.
18. Patel SS, Wong I, Johnson KA (1991) Pre-steady-state kinetic analysis of processive DNA replication including complete characterization of an exonuclease-deficient mutant. *Biochemistry* 30:511–525.
19. Ahnert P, Patel SS (1997) Asymmetric interactions of hexameric bacteriophage T7 DNA helicase with the 5′- and 3′-tails of the forked DNA substrate. *J Biol Chem* 272:32267–32273.
20. Crampton DJ, Ohi M, Qimron U, Walz T, Richardson CC (2006) Oligomeric states of bacteriophage T7 gene 4 primase/helicase. *J Mol Biol* 360:667–677.
21. Hamdan SM, et al. (2007) Dynamic DNA helicase-DNA polymerase interactions assure processive replication fork movement. *Mol Cell* 27:539–549.
22. Kumar A, et al. (2007) Model for T-antigen-dependent melting of the simian virus 40 core origin based on studies of the interaction of the beta-hairpin with DNA. *J Virol* 81:4808–4818.
23. Liu X, Schuck S, Stenlund A (2007) Adjacent residues in the E1 initiator beta-hairpin define different roles of the beta-hairpin in Ori melting, helicase loading, and helicase activity. *Mol Cell* 25:825–837.
24. Sawaya MR, Guo S, Tabor S, Richardson CC, Ellenberger T (1999) Crystal structure of the helicase domain from the replicative helicase-primase of bacteriophage T7. *Cell* 99:167–177.
25. Toth EA, Li Y, Sawaya MR, Cheng Y, Ellenberger T (2003) The crystal structure of the bifunctional primase-helicase of bacteriophage T7. *Mol Cell* 12:1113–1123.
26. Ahnert P, Picha KM, Patel SS (2000) A ring-opening mechanism for DNA binding in the central channel of the T7 helicase-primase protein. *EMBO J* 19:3418–3427.
27. Miyata T, et al. (2000) Two different oligomeric states of the RuvB branch migration motor protein as revealed by electron microscopy. *J Struct Biol* 131:83–89.
28. Enemark EJ, Joshua-Tor L (2008) On helicases and other motor proteins. *Curr Opin Struct Biol* 18:243–257.
29. Lee SJ, Qimron U, Richardson CC (2008) Communication between subunits critical to DNA binding by hexameric helicase of bacteriophage T7. *Proc Natl Acad Sci USA* 105:8908–8913.
30. Levin MK, Gurjar M, Patel SS (2005) A Brownian motor mechanism of translocation and strand separation by hepatitis C virus helicase. *Nat Struct Mol Biol* 12:429–435.
31. Patel SS, Donmez I (2006) Mechanisms of helicases. *J Biol Chem* 281:18265–18268.
32. Washington MT, Patel SS (1998) Increased DNA unwinding efficiency of bacteriophage T7 DNA helicase mutant protein 4A′/E348K. *J Biol Chem* 273:7880–7887.
33. Dong F, Weitzel SE, Von Hippel PH (1996) A coupled complex of T4 DNA replication helicase (gp41) and polymerase (gp43) can perform rapid and processive DNA strand-displacement synthesis. *Proc Natl Acad Sci USA* 93:14456–14461.
34. Kim S, Dallmann HG, McHenry CS, Marians KJ (1996) Coupling of a replicative polymerase and helicase: A tau-DnaB interaction mediates rapid replication fork movement. *Cell* 84:643–650.
35. Johnson DS, Bai L, Smith BY, Patel SS, Wang MD (2007) Single-molecule studies reveal dynamics of DNA unwinding by the ring-shaped T7 helicase. *Cell* 129:1299–309.
36. Satapathy AK, Crampton DJ, Beauchamp BB, Richardson CC (2009) Promiscuous usage of nucleotides by the DNA helicase of bacteriophage T7: Determinants of nucleotide specificity. *J Biol Chem* 284:14286–14295.